J Appl Biotechnol Rep. 2021 June;8(2):155-163

doi 10.30491/JABR.2021.130934

Journal of
Applied Biotechnology
Reports

Original Article

A Quantitative Multivariate Microscopic Analysis for Identifying Changes of Glioblastoma Cancer Cells due to Thermochemoradiation Therapy

Ali Abasiyan[1], Ebrahim Motevalian[2*], Ali Mohammad Latifi[1], Soraya Emamgholizadeh Minaei[3]

[1]Applied Biotechnology Research Center, Baqiyatallah University of Medical Sciences, Tehran, Iran
[2]Department of Surgery, School of Medicine, Baqiyatallah Hospital, Baqiyatallah University of Medical Sciences, Tehran, Iran
[3]Department of Medical Physics and Imaging, Urmia University of Medical Sciences, Urmia, Iran

Corresponding Author: Ebrahim Motevalian, MD, Department of Surgery, School of Medicine, Baqiyatallah Hospital, Baqiyatallah University of Medical Sciences, Tehran, Iran. Tel: +98-2187555380, Email: Motevalian.e@gmail.com

Received December 12, 2019; **Accepted** February 12, 2020; **Online Published** May 24, 2021

Abstract

Introduction: Although radiation is recognized as the most effective nonsurgical treatment, the outcomes and control rates are generally poor. However, a combination of radiation therapy with hyperthermia and chemotherapy can improve the efficacy of treatment. The aim was to explore the potential of morphological and gradient-based features on microscopic images in improving the identification accuracy of subtle differences in cell structure during different treatments.

Materials and Methods: Fifty single-cell images were used for each group and treatment regimen. The groups were individually subjected to: (1) hyperthermia at 43°C; (2) temozolomide (TMZ) chemotherapy at 10% inhibitory concentration; (3) radiotherapy at 2 Gy; (4) combination of TMZ chemotherapy and hyperthermia; (5) combination of radiotherapy and hyperthermia; (6) combination of TMZ chemotherapy and radiotherapy; and (7) combination of TMZ chemotherapy, radiotherapy, and hyperthermia. Morphological and gradient-based features were extracted from each cell. The area under the receiver operating characteristic (ROC) curve (AUC) was calculated for each significant feature to evaluate the performance of cell change detection.

Results: According to AUCs, gradient-based features showed superior performance to morphological features in identifying cell changes during all treatment regimens in all groups. In this regard, the AUC of the gradient-mean feature exceeded 0.599 for all groups. The ratio of maximum to minimum cell diameter was the best morphological feature, with an AUC above 0.588 for all groups.

Conclusions: Quantitative analysis of features is a reliable indicator of damage, with the potential to characterize cell changes during treatment regimens.

Keywords: Computer-Assisted, Diagnosis, Hyperthermia, Radiation Therapy, Temozolomide Chemotherapy

Citation: Abasiyan A, Motevalian E, Latifi AM, Emamgholizadeh Minaei S. A Quantitative Multivariate Microscopic Analysis for Identifying Changes of Glioblastoma Cancer Cells due to Thermochemoradiation Therapy. J Appl Biotechnol Rep. 2021;8(2):155-163. doi:10.30491/JABR.2021.130934.

Introduction

According to the World Health Organization (WHO), glioblastoma multiforme is the most common and aggressive primary tumor of the central nervous system.[1] Although radiation is recognized as the most effective nonsurgical treatment, the outcomes and control rates are generally poor. However, a combination of radiation therapy with hyperthermia and chemotherapy can improve the efficacy of treatments.[2-4]

Temozolomide (TMZ) is an effective alkylating antiglioblastoma agent with good penetration into brain tissues. It has been proven that TMZ chemotherapy has improved the survival of patients from 12 months (radiation alone) to 14.6 months (combined treatment).[5] In hyperthermia therapy, the tissue temperature increases to 41-45°C, and cellular function changes by inhibiting proliferation and repair enzymes and altering DNA conformation. In addition, hyperthermia affects the synthesis of nucleic acids, which can promote apoptosis.[6,7]

In literature, many studies have reported that radiotherapy, hyperthermia, and chemotherapy have the potential to induce structural and shape changes in glioblastoma cells. These changes include membrane blebbing, protein denaturation in the nuclear matrix, development of croissant-shaped nuclei, loss of spherical shape, increased cell irregularity, abundant cytoplasm, necrosis, and nuclei with condensed chromatin; these changes are correlated with cytotoxicity and cell damage. These studies have also evaluated cell changes after treatment using microscopic images.[8-14] Morphological and structural changes of cells can affect the gray-level intensity distribution of microscopic images. These changes can be interpreted both qualitatively (by the human eye) and quantitatively (mathematical computation). Overall, it is advantageous to determine the potential of these gray-level intensity changes in cells as a quantitative marker for the assessment of cell damage.

Several techniques, such as colony assay, flow cytometry, MTT assay, and cytogenetic analysis, have been introduced to measure cell damage. Although these techniques are effective in

evaluating cell damage after treatment, they are both expensive and time-consuming. It seems that a fast and cost-effective technique is required to assess the cells after treatment. The aim of the present study was to evaluate the potential of quantitative analysis of changes in C6 glioblastoma cell line on microscopic images during radiotherapy, hyperthermia, and chemotherapy. To the best of our knowledge, this is the first study to extract quantitative texture and morphological parameters for the prediction of cell damage following these treatment regimens.

Materials and Methods

Cell Culture and Treatment

In this experimental study, the C6 glioblastoma cell line was cultured in Dulbecco's Modified Eagle's Medium (DMEM), supplemented with 10% fetal bovine serum (FBS), 100 units/mL of penicillin, and 100 mg/mL of streptomycin. The cell line was grown as a monolayer at a density of 10^4 cells/cm^2 in T-25 cell culture flasks and kept in a humidified incubator at 37°C (5% CO_2 and 95% air).

In this study, seven cell culture flasks were prepared for different treatments: (1) localized radiofrequency (RF) hyperthermia, i.e., alternating magnetic field-activated hyperthermia at a frequency of 13.56 MHz to reach 43°C (HT); (2) TMZ chemotherapy at 10% inhibitory concentration during 24 hours of incubation (TMZ); (3) radiotherapy with 6-MV X-ray beams at the radiation dose of 2 Gy (RT); (4) TMZ chemotherapy, followed by hyperthermia therapy (HTMZ); (5) radiotherapy at a dose of 2 Gy, followed by hyperthermia (RTHT); (6) TMZ chemotherapy, followed by radiotherapy at a dose of 2 Gy (RTMZ); and (7) TMZ chemotherapy, followed by radiotherapy at a dose of 2 Gy and hyperthermia (RTMZHT). In addition, one control group (C) was prepared to compare and evaluate the effects of the treatments.

For a reliable analysis, glioblastoma cancer cells were cultured in T-25 cell culture flasks and incubated for 24 hours; then, they were treated in the groups. After treatment, the cells were trypsinized, and single-cell suspensions were floated in the culture medium. Fifty optical images were acquired using phase-contrast inverted microscopy (BEL, Monza, Italy) immediately after each treatment regimen. Finally, 400 cell images were acquired and exported in "BMP" format for further computerized image processing analysis using MATLAB (MathWorks, MA, USA). These procedures were repeated three times and the average of the results were reported.

Image Processing and Feature Extraction

Cell Segmentation

Cell segmentation was performed to remove redundant data and obtain the region of interest for further quantitative cell analysis. Some filters were required to improve the contrast of microscopic images and find the proper conditions to succeed in cell segmentation.

Contrast-limited adaptive histogram equalization (CLAHE) was used to enhance the contrast of cell images.[15] The filter was applied on small regions of the image (tiles) and was used to cut the histogram at some thresholds, followed by equalization; this process continued until all the tiles were processed and equalized. The CLAHE filter parameters were defined as follows: Number of tiles, NumTiles = [8 8]; Contrast enhancement limit, ClipLimit = 0.01; and Number of histogram bins used to build a contrast enhancing transformation, NBins = 256.

The probabilistic patch-based (PPB) filter divides the image into patches and is applied separately on each patch. The new value for each patch is calculated by weighted averaging of all patches. A shorter Euclidean distance between two patches can increase similarity and weight. Therefore, the pixels yield almost the same value for similar patches.[16] In this study, the PPB filter was used to reduce image noise and improve segmentation performance.

Although the PPB filter is an effective tool for reducing noise, it degrades the contrast resolution of the cell edge. Wavelet filter is an ideal candidate for increasing the cell edge contrast. In Wavelet filters, image signals are decomposed into two frequency channels, i.e., high-pass (H) and low-pass (L). After applying a wavelet filter, image decomposes into approximation sub-band image (LL) and detail sub-band images (LH, HL, and HH).[17] As we aimed to achieve a high-contrast resolution, the HH sub-band image (using Daubechies wavelet decomposition mother Family, db1) was considered suitable for improving the segmentation performance.

In this study, active contours proposed by Chan and Vese was used to segment the cells for further feature extraction.[18] The principle of Chan-Vese model for active contours is based on the evaluation of pixel distribution inside and outside the curve. The active contour finds the curve by minimizing the following term:

$$\int_{\text{Insidecurve}} |u_0 - c_1|^2 \, dx \cdot dy + \int_{\text{Outsidecurve}} |u_0 - c_2|^2 \, dx \cdot dy) \qquad (1)$$

where c_1 and c_2 are the mean pixel values corresponding to the inside and outside the curve, and u_0 is the pixel value in the (x, y) point. Both the Smooth Factor and Contraction Bias were set to zero for active contour segmentation. All the steps of the proposed segmentation method are illustrated in Figure 1. After successful cell segmentation, two quantitative features were extracted: (1) morphological and (2) gradient-based (texture) features.

Quantitative Features Extraction

Morphological Features

Seven morphological features were extracted from each cell: (1) ratio of major to minor diameter of the ellipse circumscribing the cell (extension); (2) ratio of perimeter to convex perimeter of the cell (convexity); (3) ratio of area to perimeter of the cell (regularity); (4) ratio of maximum to minimum diameter of the cell (aspect ratio); (5) ratio of cell area to bounding box area (form factor); (6) standard deviation of all radii of the cell (Std-radius); and (7) ratio of maximum to minimum distance between the gravity and contour of the cell (gravity factor). Figure 1 demonstrates a graphic representation of each morphological feature.

Gradient Features

The image gradient indicates the spatial grey-level intensity variations across the image. A high gradient refers to severe

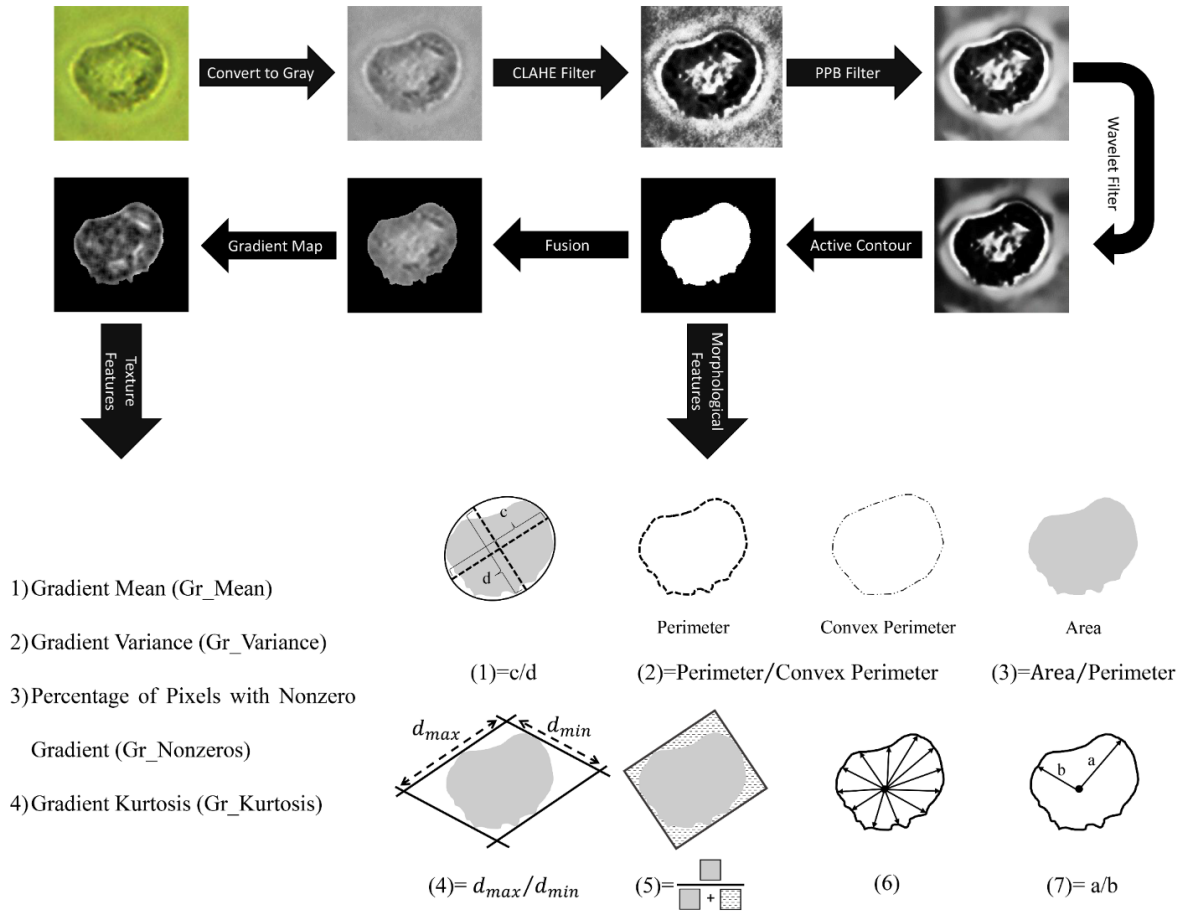

Figure 1. Overview of Image Processing Steps and Features Extraction in the Microscope Cell Image Analysis.

changes in intensity, whereas a low gradient implies smooth changes in tone. These changes can be interpreted and measured by gradient-based features. In this study, four gradient features were extracted from the cells to evaluate the intensity changes during different treatments: (1) gradient mean (Gr-mean); (2) gradient variance (Gr-variance); (3) gradient kurtosis (Gr-kurtosis); and (4) percentage of pixels with non-zero gradient (Gr-nonzero). These gradient-based features are described and measured as follows:

$$\text{Gr\_mean} = \frac{1}{M}\sum_{i,j \in \text{cell region}} G(i,j) \quad (2)$$

$$\text{Gr\_variance} = \frac{1}{M}\sum_{i,j \in \text{cell region}} \left(G(i,j) - \text{Gr\_Mean}\right)^2 \quad (3)$$

$$\text{Gr\_kurtosis} = \frac{1}{\left(\sqrt{\text{Gr\_Variance}}\right)^4}\frac{1}{M}\sum_{i,j \in \text{cell region}} \left(G(i,j) - \text{Gr\_Mean}\right)^4 - 3 \quad (4)$$

$$\text{Gr\_nonzeros} = \frac{number\ of\ G(i,j) \neq 0}{G(i,j)} \qquad i,j \in cell\ region \quad (5)$$

where G (i,j) and M represent the absolute gradient matrix and number of pixels in the cell region, respectively. A gradient map of the cell is presented in Figure 1.

Clonogenic Assay

The clonogenic assay was used to evaluate cell toxicity by considering cell reproductive death as an endpoint. After treatment, cell viability was evaluated using trypan blue dye exclusion assay. Then, single cells were seeded in 60-mm Petri dishes, containing the culture medium and 10% FBS and incubated at 37°C with 5% CO_2 in a humidified incubator. After six days, the colonies were counted using an inverted phase microscope (BEL, Monza, Italy). The plating efficiency and surviving fraction were also determined by the following equations:

$$\text{PE}(\%) = \frac{\text{Number of colonies counted}}{\text{Number of cells seeded}} \times 100 \quad (6)$$

$$\text{Surviving fraction} = \frac{\text{Colonies counted}}{\text{Cells seeded} \times \left(\frac{\text{PE}}{100}\right)} \quad (7)$$

Statistical Analysis and Classification

The cell data were tested for normality using Kolmogorov–Smirnov test. One-way analysis of variance (ANOVA) was used to determine differences in quantitative features extracted from the cells between the groups. Turkey's post hoc test was also applied to compare significant features between the groups. *P* value less than 0.05 was considered significant. The area under the receiver operating characteristic (ROC) curve (AUC) was

calculated for each significant feature in the groups to evaluate classification performance. The AUC values were estimated at 95% confidence interval. All statistical analyses were performed using SPSS version 19.

Results

Surviving Fraction of C6 Cells

Table 1 demonstrates the surviving fraction of the cells during different treatment regimens. As compared to the non-treated control group, survival fraction of HT, TMZ chemotherapy and RT groups decreased to 9%, 16% and 36%, respectively. HT in combination with TMZ chemotherapy or RT showed 15% and 36% reduction in survival fraction compared to HT alone, respectively. In addition, a combination of RT and TMZ chemotherapy had a lower survival fraction in comparison with the other two combined treatments (Survival fraction of RTMZ vs. HTMZ vs. RTHT: 46% vs. 76% vs. 55%). Finally, a combination of three treatment modalities could induce the highest cell damage and had the lowest survival fraction (29%). To confirm the proposed method, all the results were compared with the surviving fraction.

Table 1. Effects of Different Treatment Regimens on Colony Formation Ability

Treatment	Survival Fraction
Control	1.00
HT	0.91
TMZ	0.84
RT	0.64
HTMZ	0.76
RTHT	0.55
RTMZ	0.46
RTMZHT	0.29

HT: Hyperthermia, TMZ: Temozolomide, RT: Radiotherapy, HTMZ: TMZ chemotherapy + hyperthermia therapy, RTHT: Radiotherapy + Hyperthermia, RTMZ: TMZ chemotherapy + Radiotherapy, RTMZHT: TMZ chemotherapy + Radiotherapy + Hyperthermia.

Morphological Changes After Treatment

Figure 2 presents the images of C6 glioblastoma cell line after different treatment regimens. The diagnostic performance of morphological parameters in differentiation between the treatment regimens is presented in Table 2. Since the highest cell damage (the lowest survival fraction of cell) belonged to the RTMZHT treatment, all morphological parameters could differentiate between the control and RTMZHT groups with an AUC of 1. The diagnostic ability of morphological parameters decreased by reducing the differences in survival fraction of cells. Hence, distinguish performances of morphological parameters were below one between the control and the other treatment groups. In this regard, the worst performance was attributed to convexity in classification of control and HT groups with an AUC of 0.571.

The same trend was seen for classifying treatment groups. Thus, groups with higher differences in survival fraction (cell damage) had a higher classification performance. As it can be seen in Table 1, the highest differences of survival fraction between treatment groups belonged to HT and RTMZHT. Therefore, the classification performance between HT and RTMZHT was higher than the other groups (AUC range: 0.978-1). According to AUC, the best and worst morphological parameter for classification tasks were aspect_ratio and convexity, respectively (Table 2).

Gradient Changes After Treatment

Like morphological parameters, the same trend was seen for gradient parameters between classification performance and clonogenic assay results (Table 3). In this regard, all the gradient parameters could differentiate between the control and RTMZHT groups (AUC, 1). In classification of control and other treatment groups, diagnostic performance of all parameters was lower, which AUC was in the range of 0.555 to 0.951. The worst performance was attributed to Gr_Kurtosis in the classification

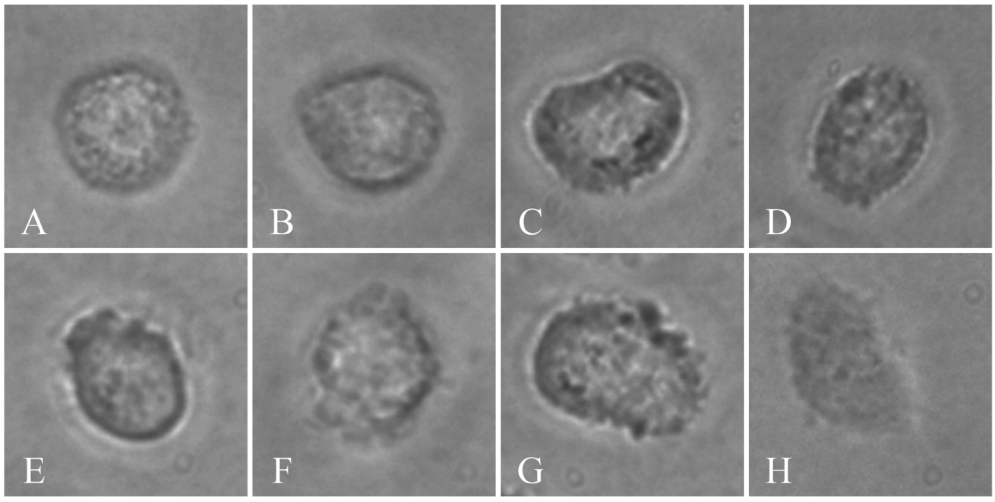

Figure 2. Sample of Gray-Scale Optical Microscope Images of Glioblastoma C6 Cell Line After Different Treatment Regimens: A) control; B) hyperthermia; C) temozolomide; D) radiation; E) temozolomide + hyperthermia; F) radiation+ hyperthermia; G) temozolomide + radiation; H) temozolomide + radiation + hyperthermia; All of the microscope images were obtained with 400X magnification.

Table 2. Summary of Performance for Significant Morphological Features in Different Treatment and Associated AUC* Values

Groups	Extension	Convexity	Regularity	Aspect_ratio	Form_factor	Std_rad	Grav_factor
C&HT	0.581 (0.475, 0.686)	0.571 (0.466, 0.76)	0.579 (0.477, 0.686)	0.588 (0.483, 0.694)	0.579 (0.471, 0.687)	0.579 (0.475, 0.684)	0.586 (0.482, 0.690)
C&TMZ	0.642 (0.563 0.721)	0.607 (0.623, 0.791)	0.613 (0.532, 0.694)	0.660 (0.587, 0.734)	0.638 (0.560, 0.715)	0.627 (0.549, 0.705)	0.656 (0.542, 0.770)
C&RT	0.785 (0.768, 0.802)	0.732 (0.667, 0.796)	0.754 (0.719, 0.790)	0.788 (0.771, 0.805)	0.770 (0.743, 0.796)	0.757 (0.717, 0.796)	0.788 (0.771, 0.795)
C&HTMZ	0.737 (0.692, 0.783)	0.704 (0.649, 0.860)	0.708 (0.652, 0.764)	0.779 (0.754, 0.800)	0.728 (0.679, 0.776)	0.719 (0.650, 0.789)	0.765 (0.734, 0.795)
C&RTHT	0.798 (0.795, 0.805)	0.755 (0.710, 0.800)	0.782 (0.750, 0.816)	0.812 (0.794, 0.830)	0.793 (0.781, 0.805)	0.789 (0.762, 0.816)	0.799 (0.770, 0.828)
C&RTMZ	0.898 (0.855, 0.941)	0.830 (0.790, 0.870)	0.834 (0.901,0.967)	0.939 (0.917, 0.961)	0.895 (0.887, 0.900)	0.860 (0.816, 0.904)	0.920 (0.852, 0.987)
C&RTMZHT	1.000	1.000	1.000	1.000	1.000	1.000	1.000
HT&TMZ	0.581 (0.488, 0.694)	0.557 (0.450, 0.664)	0.572 (0.467, 0.677)	0.610 (0.621, 0.699)	0.581 (0.477, 0.686)	0.579 (0.475, 0.684)	0.600 (0.595, 0.704)
HT&RT	0.737 (0.666, 0.847)	0.726 (0.647, 0.804)	0.728 (0.574, 0.882)	0.769 (0.688, 0.850)	0.736 (0.689, 0.783)	0.735 (0.689, 0.781)	0.753 (0.676, 0.830)
HT&HTMZ	0.640 (0.591, 0.689)	0.594 (0.507, 0.681)	0.628 (0.548, 0.707)	0.664 (0.598, 0.739)	0.632 (0.588, 0.676)	0.630 (0.551, 0.709)	0.650 (0.577, 0.723)
HT&RTHT	0.779 (0.755, 0.800)	0.742 (0.692, 0.791)	0.746 (0.704, 0.789)	0.785 (0.769, 0.801)	0.771 (0.733, 0.809)	0.747 (0.694, 0.800)	0.780 (0.755, 0.805)
HT&RTMZ	0.794 (0.785, 0.803)	0.780 (0.742, 0.818)	0.785 (0.768, 0.802)	0.820 (0.782, 0.858)	0.793 (0.778, 0.809)	0.790 (0.778, 0.803)	0.795 (0.787, 0.803)
HT&RTMZHT	1.000	0.978 (0.951, 1.000)	0.980 (0.963, 1.000)	1.000	0.999 (0.997, 1.000)	0.984 (0.967, 1.000)	1.000
TMZ&RT	0.730 (0.650, 0.809)	0.704 (0.615, 0.793)	0.710 (0.653, 0.768)	0.751 (0.706, 0.797)	0.728 (0.675, 0.781)	0.725 (0.676, 0.774)	0.731 (0.650, 0.813)
TMZ&HTMZ	0.593 (0.490, 0.596)	0.561 (0.455, 0.667)	0.572 (0.446, 0.680)	0.626 (0.522, 0.730)	0.585 (0.481, 0.690)	0.577 (0.473, 0.682)	0.602 (0.500, 0.703)
TMZ&RTHT	0.759 (0.707, 0.800)	0.734 (0.779, 0.889)	0.736 (0.676, 0.797)	0.772 (0.716, 0.829)	0.747 (0.688, 0.806)	0.741 (0.675, 0.806)	0.770 (0.764, 0.777)
TMZ&RTMZ	0.780 (0.739, 0.861)	0.752 (0.742, 0.761)	0.762 (0.727, 0.797)	0.798 (0.792, 0.800)	0.774 (0.734, 0.815)	0.768 (0.741, 0.785)	0.787 (0.770, 0.800)
TMZ&RTMZHT	0.996 (0.990, 1.000)	0.948 (0.917, 0.985)	0.960 (0.924, 0.997)	1.000	0.990 (0.981, 1.000)	0.961 (0.929, 0.992)	1.000
RT&HTMZ	0.691 (0.584, 0.799)	0.594 (0.489, 0.699)	0.601 (0.498, 0.704)	0.695 (0.493, 0.697)	0.659 (0.550, 0.767)	0.618 (0.516, 0.721)	0.694 (0.589, 0.698)
RT&RTHT	0.607 (0.502, 0.712)	0.580 (0.495, 0.637)	0.592 (0.487, 0.698)	0.630 (0.530, 0.730)	0.596 (0.492, 0.700)	0.593 (0.487, 0.699)	0.618 (0.517, 0.720)
RT&RTMZ	0.741 (0.658, 0.825)	0.710 (0.654, 0.766)	0.718 (0.638, 0.798)	0.747 (0.661, 0.833)	0.731 (0.649, 0.814)	0.726 (0.655, 0.797)	0.745 (0.670, 0.820)
RT&RTMZHT	0.895 (0.888, 0.900)	0.866 (0.838, 0.894)	0.874 (0.849, 0.899)	0.915 (0.892, 0.938)	0.892 (0.878, 0.906)	0.882 (0.849, 0.935)	0.898 (0.823, 0.974)
HTMZ&RTHT	0.716 (0.626, 0.797)	0.677 (0.599, 0.756)	0.696 (0.630, 0.762)	0.735 (0.655, 0.815)	0.709 (0.624, 0.795)	0.700 (0.612, 0.788)	0.729 (0.657, 0.802)
HTMZ&RTMZ	0.760 (0.705, 0.815)	0.720 (0.668, 0.771)	0.737 (0.692, 0.782)	0.781 (0.724, 0.839)	0.754 (0.692, 0.816)	0.745 (0.699, 0.791)	0.770 (0.649, 0.890)
HTMZ&RTMZHT	0.920 (0.893,0.947)	0.893 (0.838, 0.948)	0.909 (0.855, 0.963)	0.933 (0.775, 0.891)	0.912 (0.874,0.950)	0.912 (0.835, 0.989)	0.921 (0.891, 0.951)
RTHT& RTMZ	0.601 (0.499, 0.703)	0.573 (0.464, 0.682)	0. 579 (0.473, 0.685)	0.632 (0.531, 0.732)	0.580 (0.474, 0.686)	0.579 (0.474, 0.684)	0.612 (0.508, 0.716)
RTHT&RTMZHT	0.782 (0.576, 0.787)	0.704 (0.620, 0.788)	0.713 (0.617, 0.810)	0.830 (0.780, 0.880)	0.766 (0.681, 0.851)	0.755 (0.719, 0.790)	0.816 (0.732, 0.889)
RTMZ&RTMZHT	0.739 (0.663, 0.815)	0.652 (0.541, 0.763)	0.693 (0.597, 0.790)	0.773 (0.684, 0.863)	0.712 (0.621, 0.802)	0.706 (0.621, 0.790)	0.762 (0.696, 0.829)

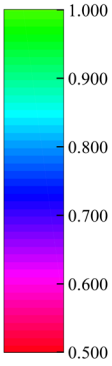

AUC= area under ROC curve; * Numbers in parentheses are 95% confidence intervals.

Table 3. Summary of Performance for Significant Gradient Features in Different Treatment and Associated AUC* values.

Groups	Gr_Mean	Gr_Variance	Gr_NonZeros	Gr_Kurtosis
C&HT	0.599 (0.496, 0.701)	0.571 (0.458, 0.684)	0.563 (0.459, 0.667)	0.555 (0.440, 0.670)
C&TMZ	0.684 (0.607, 0.761)	0.594 (0.483, 0.705)	0.580 (0.476, 0.683)	0.576 (0.471, 681)
C&RT	0.890 (0.878, 0.902)	0.857 (0.682, 0.833)	0.830 (0.781, 0.879)	0.798 (0.728, 0.871)
C&HTMZ	0.840 (0.791, 0.889)	0.760 (0.823, 0.897)	0.754 (0.674, 0.834)	0.737 (0.684, 0.790)
C&RTHT	0.898 (0.893, 0.903)	0.888 (0.874, 0.902)	0.868 (0.835, 0.901)	0.857 (0.823, 0.891)
C&RTMZ	0.951 (0.901, 0.991)	0.909 (0.893, 0.925)	0.892 (0.860, 0.924)	0.876 (0.858, 0.894)
C&RTMZHT	1.000	1.000	1.000	1.000
HT&TMZ	0.613 (0.499, 0.727)	0.571 (0.463, 0.685)	0.550 (0.435, 0.665)	0.546 (0.441, 651)
HT&RT	0.855 (0.819, 0.891)	0.828 (0.797, 0.919)	0.813 (0.740, 0.887)	0.788 (0.752, 0.824)
HT&HTMZ	0.667 (0.666, 0.868)	0.649 (0.458, 0.740)	0.623 (0.624, 0.822)	0.604 (0.522, 0.686)
HT&RTHT	0.851 (0.814, 0.889)	0.840 (0.808, 0.872)	0.835 (0.789, 0.881)	0.819 (0.776, 0.863)
HT&RTMZ	0.898 (895, 0.905)	0.861 (0.843, 0.879)	0.849 (0.813, 0.886)	0.826 (0.808, 0.854)
HT&RTMZHT	1.000	1.000	1.000	0.991 (0.982, 1.000)
TMZ&RT	0.754 (0.679, 0.830)	0.740 (0.668, 0.812)	0.717 (0.645, 0.789)	0.705 (0.613, 0.798)
TMZ&HTMZ	0.672 (0.569, 0.775)	0.592 (0.490, 0.694)	0.580 (0.478, 0.682)	0.560 (0.451, 0.669)
TMZ&RTHT	0.827 (0.745, 0.909)	0.811 0.759, 0.864)	0.796 (0.735, 0.857)	0.763 (0.689, 0.837)
TMZ&RTMZ	0.851 (0.831, 0.871)	0.832 (0.801, 0.863)	0.812 (0.774, 0.849)	0.806 (0.755, 0.857)
TMZ&RTMZHT	1.000	1.000	1.000	0.982 (0.972, 0.992)
RT&HTMZ	0.696 (0.595, 0.776)	0.668 (0.564, 0.772)	0.628 (0.476, 0.701)	0.614 (0.509, 0.718)
RT&RTHT	0.657 (0.552, 0.762)	0.595 (0.491, 0.699)	0.586 (0.482, 0.690)	0.570 (0.466, 0.674)
RT&RTMZ	0.801 (0.737, 0.864)	0.781 (0.700, 0.763)	0.746 (0.663, 0.829)	0.730 (0.643, 0.817)
RT&RTMZHT	0.919 (0.887, 0.931)	0.898 (0.883, 0.913)	0.891 (0.871, 0.921)	0.868 (0.841, 0.895)
HTMZ&RTHT	0.782 (0.719, 0.845)	0.747 (0.658, 0.836)	0.733 (0.655, 0.811)	0.711 (0.629, 0.793)
HTMZ&RTMZ	0.843 (0.808, 0.878)	0.806 (0.750, 0.862)	800 (0.737, 0.864)	0.783 (0.731, 0.834)
HTMZ&RTMZHT	0.940 (0.916, 0.974)	0.919 (0.886, 0.942)	0.898 (0.865, 0.931)	0.891 (0.871, 0.911)
RTHT& RTMZ	0.680 (0.577, 0.783)	0.639 (0.494, 0.704)	0.653 (0.549, 0.757)	0.596 (0.490, 0.702)
RTHT&RTMZHT	0.864 (0.841, 0.888)	0.828 (0.805, 0.851)	0.816 (0.761, 0.872)	0.808 (0.764, 0.851)
RTMZ&RTMZHT	0.799 (0.741, 0.856)	0.761 (0.790, 0.822)	0.727 (0.646, 0.807)	0.709 (0.645, 0.773)

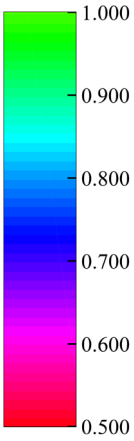

AUC= area under ROC curve; * Numbers in parentheses are 95% confidence intervals.

of control and HT groups with AUC of 0.555.

In classification of treatment groups, the best performance was achieved for classification between HT and RTMZHT and between TMZ and RTMZHT with AUC of 1 for Gr_Mean, Gr_Variance, and Gr_NonZeros parameters. Also, the worst performance was attributed to Gr-kurtosis in the classification of HT and TMZ groups (AUC, 0.546). Other classification performances for different treatment regimens are indicated in Table 3. On the other hand, with respect to individual gradient-based parameters, Gr-mean was superior to others, as it showed the highest AUC in the classification of different treatment groups.

Discussion

This study aimed to evaluate the diagnostic performance of quantitative features extracted from microscopic images of C6 glioblastoma cells for detecting changes during different treatments. The results indicated that morphological and gradient-based features can represent cell changes during TMZ chemotherapy, hyperthermia, and radiation therapy. According to AUCs, gradient-based (Gr-mean) features showed better performance in comparison with morphological features in identifying cell changes during all treatment regimens; the AUC of Gr-mean exceeded 0.599 in all the classification groups.

Treatment of cells with chemotherapy, hyperthermia, and radiation lead to changes in cells. TMZ is an alkylating agent that methylate O6 position of guanine in DNA.[19] Hyperthermia causes the denaturation of proteins, cell membrane changes, and induce cell apoptosis.[20] Moreover, the biological effects of ionizing radiation are due to oxidative stress, double strand break of DNA, and chromosomal aberrations[21] which can lead to cell death. These treatments cause structural, morphological, and molecular changes in the cells and the cytotoxic effects of them can be analyzed with quantitative features extracted from microscopic images.

By analyzing the trends of variation in morphological and gradient-based features, it was found that these quantitative features were consistent with the colony assay results. By increasing damage, the gradient intensity of the cells decreased and vice versa, whereas cell membrane irregularity and cell extension increased (Figure 3 and Table 1).

The results of the present study indicated that by combining different treatment regimens, the diagnostic performance of features increased. Several studies have confirmed this effect on glioblastoma cells in laboratory tests.[22-25] Considering the induced cell damage, differences in quantitative features were more distinguishable between the cell groups. For instance, regarding the aspect ratio, when TMZ chemotherapy and hyperthermia therapy were combined, AUC increased from 0.588 (HT) and 0.660 (TMZ) to 0.779 (HTMZ), respectively (Table 2). Similar trends were observed for other features and treatment regimens. The best performance was related to the classification of control and RTMZHT groups, with an AUC of one for all the morphological and gradient-based features (Table 2 and Table 3). Quantitative feature results were in complete agreement with the results of colony assay. The highest cellular damage was observed for the RTMZHT group, which had the lowest SF value (0.29).

The findings of many studies, which have qualitatively evaluated cell morphology after treatment, are not consistent with our results. Antal et al treated glioma cells with radiation (10 Gy) and did not find any significant differences in the cell irregularity index between the control and treatment groups.[12] Other studies indicated that after treatment of glioblastoma cells, they became more round and spherical in shape[8,13,26-28] which is not in line with the findings of the present study. One of the main causes of the observed discrepancy could be that the cells were bound to the dish surface in the mentioned studies. Therefore, the cells lost their correct morphology, and analysis of true shape changes during treatment was impossible. Under these conditions, the cells lose their adhesion to the dish surface after treatment, which changes their shape from extended to spherical; consequently, these changes in shape cannot be true indicators. Nevertheless, in the present study, for a reliable morphological analysis, the cells were first trypsinized and floated in the culture medium, and then, images were acquired.

Regarding the quantitative analysis, Abbasian Ardakani et al indicated that changes induced by radiation and hyperthermia

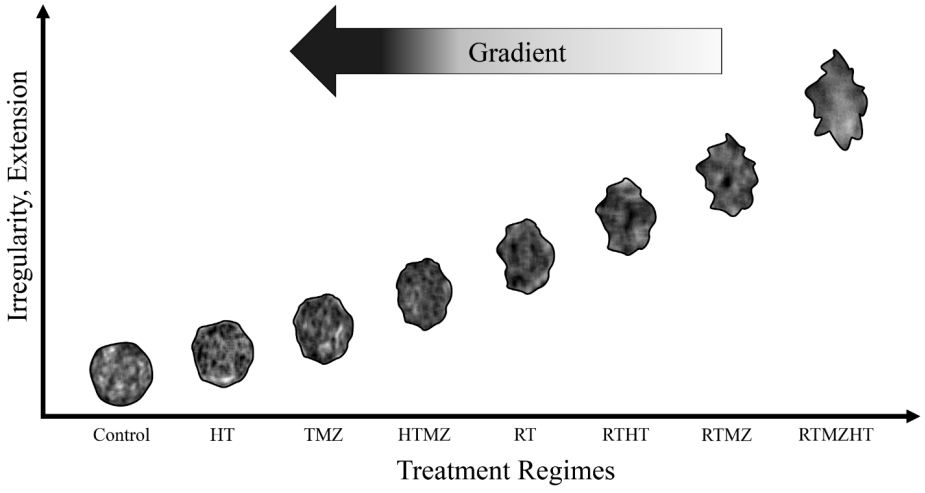

Figure 3. Schematic Trend of Cell Changes During Different Treatment Regimens.

treatments can be extracted via computerized texture analysis with high accuracy. They introduced their quantitative features as indicators for detecting cell damage.[29] The present study is the first attempt at evaluating the quantitative morphological changes of cells during treatment. Previous studies have manually assessed cell shape, which is operator-dependent and inaccurate in terms of the extracted information. In addition, visual inspection cannot detect fine and subtle changes, while computerized feature extraction and analysis can overcome this limitation. No studies were found in the literature, evaluating cell gradient changes during treatment both qualitatively and quantitatively.

The present study showed that quantitative features could identify cell changes during different treatment regimens. However, further studies with larger feature variations and different cell lines are necessary to confirm our results. In addition, since all microscopic image analyses were compared with the control group and the reference for statistical analysis, other cell characteristics were not considered as complementary information. In this study, microscope focusing adjustment was performed manually, which could influence the image texture. To reduce the impact of focusing on image features, all imaging procedures were performed by one person. Hence, the variation of texture features were minimized. Furthermore, autoexposure was applied to homogenize all images in terms of brightness and texture. The main advantage of this method is that it can be performed in a short period of time, while other techniques are either time-consuming (e.g., colony assay) or expensive (e.g., flowcytometry). Also, quantitative feature analysis does not impose any additional costs.

Conclusions

In conclusion, the proposed method seems to be useful for *in vitro* evaluation of cells after treatment using two-dimensional microscopic images. The preliminary findings indicated that microscopic quantitative analysis of cell images can be used as a complementary technique for cytogenetic examinations to characterize the cellular damages after different treatments.

Authors' Contributions

All authors contributed equally to this research.

Conflict of Interest Disclosures

The authors report no conflicts of interest.

Acknowledgments

This study was supported by the Baqiyatallah University of Medical Sciences, Tehran, Iran. We are grateful for their support.

References

1. Louis DN, Ohgaki H, Wiestler OD, et al. The 2007 WHO classification of tumours of the central nervous system. Acta Neuropathol. 2007;114(2):97-109. doi:10.1007/s00401-007-0243-4.
2. Stupp R, Hegi ME, Mason WP, et al. Effects of radiotherapy with concomitant and adjuvant temozolomide versus radiotherapy alone on survival in glioblastoma in a randomised phase III study: 5-year analysis of the EORTC-NCIC trial. Lancet Oncol. 2009;10(5):459-466. doi:10.1016/s1470-2045(09)70025-7.
3. Mahmoudi K, Bouras A, Bozec D, Ivkov R, Hadjipanayis C. Magnetic hyperthermia therapy for the treatment of glioblastoma: a review of the therapy's history, efficacy and application in humans. Int J Hyperthermia. 2018;34(8):1316-1328. doi:10.1080/02656736.2018.1430867.
4. Borasi G, Nahum A, Paulides MM, et al. Fast and high temperature hyperthermia coupled with radiotherapy as a possible new treatment for glioblastoma. J Ther Ultrasound. 2016;4:32. doi:10.1186/s40349-016-0078-3.
5. Stupp R, Mason WP, van den Bent MJ, et al. Radiotherapy plus concomitant and adjuvant temozolomide for glioblastoma. N Engl J Med. 2005;352(10):987-996. doi:10.1056/NEJMoa043330.
6. Yi GQ, Gu B, Chen LK. The safety and efficacy of magnetic nano-iron hyperthermia therapy on rat brain glioma. Tumour Biol. 2014;35(3):2445-2449. doi:10.1007/s13277-013-1324-8.
7. Wang DC, Zhang Y, Chen HY, et al. Hyperthermia promotes apoptosis and suppresses invasion in C6 rat glioma cells. Asian Pac J Cancer Prev. 2012;13(7):3239-3245. doi:10.7314/apjcp.2012.13.7.3239.
8. Jinno-Oue A, Shimizu N, Hamada N, et al. Irradiation with carbon ion beams induces apoptosis, autophagy, and cellular senescence in a human glioma-derived cell line. Int J Radiat Oncol Biol Phys. 2010;76(1):229-241. doi:10.1016/j.ijrobp.2009.08.054.
9. Zhuang W, Li B, Long L, Chen L, Huang Q, Liang Z. Induction of autophagy promotes differentiation of glioma-initiating cells and their radiosensitivity. Int J Cancer. 2011;129(11):2720-2731. doi:10.1002/ijc.25975.
10. Hildebrandt B, Wust P, Ahlers O, et al. The cellular and molecular basis of hyperthermia. Crit Rev Oncol Hematol. 2002;43(1):33-56. doi:10.1016/s1040-8428(01)00179-2.
11. Jakubowicz-Gil J, Langner E, Bądziul D, Wertel I, Rzeski W. Apoptosis induction in human glioblastoma multiforme T98G cells upon temozolomide and quercetin treatment. Tumour Biol. 2013;34(4):2367-2378. doi:10.1007/s13277-013-0785-0.
12. Antal O, Hackler L Jr, Shen J, et al. Combination of unsaturated fatty acids and ionizing radiation on human glioma cells: cellular, biochemical and gene expression analysis. Lipids Health Dis. 2014;13:142. doi:10.1186/1476-511x-13-142.
13. Teodori L, Albertini MC, Uguccioni F, et al. Static magnetic fields affect cell size, shape, orientation, and membrane surface of human glioblastoma cells, as demonstrated by electron, optic, and atomic force microscopy. Cytometry A. 2006;69(2):75-85. doi:10.1002/cyto.a.20208.
14. Chen F, Wang D. Inhibition of glioblastoma growth and invasion by 125I brachytherapy in rat glioma model. Am J Transl Res. 2017;9(5):2243-2254.
15. Reza AM. Realization of the contrast limited adaptive histogram equalization (CLAHE) for real-time image enhancement. J VLSI Signal Process Syst Signal Image Video Technol. 2004;38(1):35-44. doi:10.1023/b:vlsi.0000028532.53893.82.
16. Deledalle CA, Denis L, Tupin F. Iterative weighted maximum likelihood denoising with probabilistic patch-based weights. IEEE Trans Image Process. 2009;18(12):2661-2672. doi:10.1109/tip.2009.2029593.
17. Broughton SA, Bryan K. Discrete Fourier Analysis and Wavelets: Applications to Signal and Image Processing. John Wiley & Sons; 2018.
18. Chan TF, Vese LA. Active contours without edges. IEEE Trans Image Process. 2001;10(2):266-277. doi:10.1109/83.902291.
19. Hsu SPC, Kuo JS, Chiang HC, et al. Temozolomide, sirolimus and chloroquine is a new therapeutic combination that

synergizes to disrupt lysosomal function and cholesterol homeostasis in GBM cells. Oncotarget. 2018;9(6):6883-6896. doi:10.18632/oncotarget.23855.

20. Roti Roti JL. Cellular responses to hyperthermia (40-46 degrees C): cell killing and molecular events. Int J Hyperthermia. 2008;24(1):3-15. doi:10.1080/02656730701769841.
21. Reisz JA, Bansal N, Qian J, Zhao W, Furdui CM. Effects of ionizing radiation on biological molecules--mechanisms of damage and emerging methods of detection. Antioxid Redox Signal. 2014;21(2):260-292. doi:10.1089/ars.2013.5489.
22. Ohtake M, Umemura M, Sato I, et al. Hyperthermia and chemotherapy using Fe(Salen) nanoparticles might impact glioblastoma treatment. Sci Rep. 2017;7:42783. doi:10.1038/srep42783.
23. Rezaie P, Khoei S, Khoee S, Shirvalilou S, Mahdavi SR. Evaluation of combined effect of hyperthermia and ionizing radiation on cytotoxic damages induced by IUdR-loaded PCL-PEG-coated magnetic nanoparticles in spheroid culture of U87MG glioblastoma cell line. Int J Radiat Biol. 2018;94(11):1027-1037. doi:10.1080/09553002.2018.1495855.
24. Man J, Shoemake JD, Ma T, et al. Hyperthermia sensitizes glioma stem-like cells to radiation by Inhibiting AKT signaling. Cancer Res. 2015;75(8):1760-1769. doi:10.1158/0008-5472.can-14-3621.
25. Babincová M, Vrbovská H, Sourivong P, Babinec P, Durdík Š. Application of albumin-embedded magnetic nanoheaters for release of etoposide in integrated chemotherapy and hyperthermia of U87-MG glioma cells. Anticancer Res. 2018;38(5):2683-2690. doi:10.21873/anticanres.12510.
26. Colen CB, Seraji-Bozorgzad N, Marples B, Galloway MP, Sloan AE, Mathupala SP. Metabolic remodeling of malignant gliomas for enhanced sensitization during radiotherapy: an in vitro study. Neurosurgery. 2006;59(6):1313-1323. doi:10.1227/01.neu.0000249218.65332.bf.
27. Hirose Y, Berger MS, Pieper RO. p53 effects both the duration of G2/M arrest and the fate of temozolomide-treated human glioblastoma cells. Cancer Res. 2001;61(5):1957-1963.
28. Shen W, Hu JA, Zheng JS. Mechanism of temozolomide-induced antitumour effects on glioma cells. J Int Med Res. 2014;42(1):164-172. doi:10.1177/0300060513501753.
29. Abbasian Ardakani A, Rajaee J, Khoei S. Diagnosis of human prostate carcinoma cancer stem cells enriched from DU145 cell lines changes with microscopic texture analysis in radiation and hyperthermia treatment using run-length matrix. Int J Radiat Biol. 2017;93(11):1248-1256. doi:10.1080/09553002.2017.1359429.